www.elsevier.com/locate/talanta

An interferometric imaging biosensor using weighted spectrum analysis to confirm DNA monolayer films with attogram sensitivity

Rongxin Fu, Qi Li, Ruliang Wang, Ning Xue, Xue Lin, Ya Su, Kai Jiang, Xiangyu Jin, Rongzan Lin, Wupeng Gan, Ying Lu, Guoliang Huang

PII: S0039-9140(17)31263-8
DOI: https://doi.org/10.1016/j.talanta.2017.12.066
Reference: TAL18202

To appear in: *Talanta*

Received date: 28 August 2017
Revised date: 13 December 2017
Accepted date: 21 December 2017

Cite this article as: Rongxin Fu, Qi Li, Ruliang Wang, Ning Xue, Xue Lin, Ya Su, Kai Jiang, Xiangyu Jin, Rongzan Lin, Wupeng Gan, Ying Lu and Guoliang Huang, An interferometric imaging biosensor using weighted spectrum analysis to confirm DNA monolayer films with attogram sensitivity, *Talanta,* https://doi.org/10.1016/j.talanta.2017.12.066

An interferometric imaging biosensor using weighted spectrum analysis to confirm DNA monolayer films with attogram sensitivity

Rongxin Fu[a1], Qi Li[a1], Ruliang Wang[a], Ning Xue[a], Xue Lin[a], Ya Su[a], Kai Jiang[a], Xiangyu Jin[a], Rongzan Lin[a], Wupeng Gan[b],Ying Lu[a], Guoliang Huang[a,b*]

*

[a]Department of Biomedical Engineering, the School of Medicine, Tsinghua University, Beijing, 100084, China.

[b]National Engineering Research Center for Beijing Biochip Technology, Beijing, 102206, China.

*Corresponding author. tshgl@tsinghua.edu.cn

Abstract:

Interferometric imaging biosensors are powerful and convenient tools for confirming the existence of DNA monolayer films on silicon microarray platforms. However, their accuracy and sensitivity need further improvement because DNA molecules contribute to an inconspicuous interferometric signal both in thickness and size. Such weaknesses result in poor performance of these biosensors for low DNA content analyses and point mutation tests. In this paper, an interferometric imaging biosensor with weighted spectrum analysis is presented to confirm DNA monolayer films. The interferometric signal of DNA molecules can be extracted and then quantitative detection results for DNA microarrays can be reconstructed. With the proposed strategy, the relative error of thickness detection was reduced from 88.94% to merely 4.15%. The mass sensitivity per unit area of the proposed biosensor reached 20 attograms (ag). Therefore, the sample consumption per unit area of the target DNA content was only 62.5 zeptomoles (zm), with the volume of 0.25 picolitres

[1] These authors contributed equally to this work.

(pL). Compared with the fluorescence resonance energy transfer (FRET), the measurement veracity of the interferometric imaging biosensor with weighted spectrum analysis is free to the changes in spotting concentration and DNA length. The detection range was more than 1 μm. Moreover, single nucleotide mismatch could be pointed out combined with specific DNA ligation. A mutation experiment for lung cancer detection proved the high selectivity and accurate analysis capability of the presented biosensor.

Graphical abstract

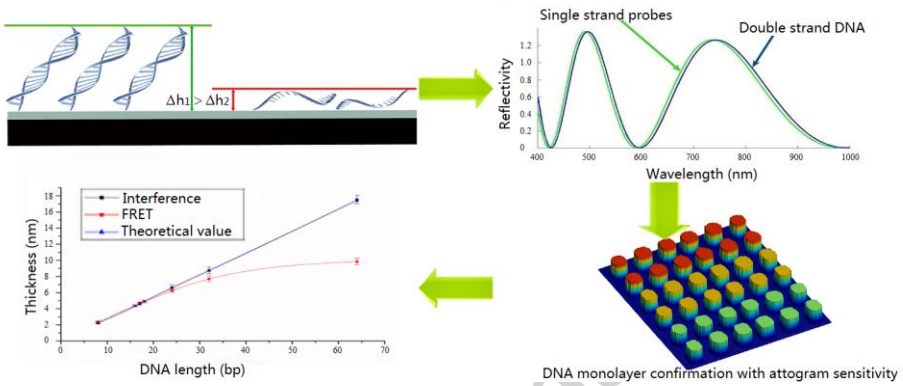

Keywords: Interferometric biosensor; Attogram sensitivity; Sub-nanoscale accuracy; Point mutation detection

1. INTRODUCTION

Label-free detection of DNA is a sought after technique due to the ever increasing demand for specific recognition of DNA sequence in the fields of expression screening, medical examination, and drug discovery [1,2]. Compared to traditional fluorescence-based methods, label-free techniques offer quantitative measurement of DNA interactions without fluorescent labeling [3].

Thus, label-free DNA detection techniques are especially investigated as they eliminate the necessity for complicated functionalization processes and expensive fabrication costs [4].

Among the many label-free DNA detection techniques, interferometric imaging biosensors have generated extensive attention and interest [5-7]. Combined with DNA microarray technology, this method can confirm DNA molecules by detecting the interference signals of DNA monolayer films on silicon-based microarray platforms with high repeatability and throughput [8,9]. Merely amino modification or similar simple immobilization and ordinary interference optical setups can support the detection process. Meanwhile, modified gold nanoparticles or other additional markers are not necessary, so complex chemical operations are not needed [8]. Thus, DNA molecules retain their intrinsic physicochemical properties. Moreover, interferometric imaging biosensors do not rely on novel nanomaterials, so the detection process is inexpensive and simple to perform [7]. However, the accuracy and sensitivity of these biosensors need further improvement, which imposes restrictions on their medical and clinical applications. The thicknesses of DNA monolayer films measured by interferometric imaging biosensors tend to be thinner than the true values. Lev Moiseev et al. [10] measured the layer heights of DNA films on a silicon surface by both fluorescence self-interference and interferometric imaging and found that the thicknesses measured by interferometric imaging were much thinner. Such a poor accuracy makes interferometric imaging biosensors unsuitable for precise conformation analysis so specific DNA ligation for point mutation testing could not be detected. Additionally, according to previous publications [11], interferometric imaging detection is usually performed with a > 20 μM DNA concentration, and the hybridization process is conducted by immersing the biosensors into target DNA solutions of > 100 μL [12]. This large sample consumption renders the detection limit and

sensitivity quite poor compared to fluorescent methods or other complicated chemical sensors [13]. The main reason for these deficiencies is that only a minimal portion of the substrates are equipped with double-stranded DNA molecules. DNA molecules tend to lie randomly on the silicon-based chip, so the interference variation is too little to detect [10]. The interferometric signal of DNA molecules is often masked by the silicon substrates and the probes.

Here, an interferometric imaging biosensor is presented to confirm DNA monolayer films with attogram sensitivity and detect single point mutation. Compared with other interferometric imaging biosensors, the fundamental differences lie in three aspects. First, the inherent tilt properties of double-strand DNA molecules were exploited to generate thicker monolayer films and enhance the detection sensitivity. Next, weighted spectrum analysis method was presented to extract the interferometric signal of DNA molecules and measure the thickness variation accurately. Moreover, combined with specific DNA ligation, single nucleotide mismatch could be pointed out firstly with interferometric imaging biosensors. With these strategies, an integrated microarray biosensor and supporting optical setup was proposed. The proposed biosensor possesses several advantages over current interferometric imaging biosensors, including measurement precision, detection sensitivity, and strong response for single nucleotide mismatch, making it an appealing solution for disease diagnosis, mutation screening, virus detection, medical examination, etc. [5-9,14]. A mutation experiment for lung cancer detection proved the high selectivity and accurate analysis capability of the presented biosensor.

2. MATERIALS AND METHODS

In the experimental part, we designed and conducted four experiments. First, the weighted spectrum analysis algorithm was compared with three current methods, proving the proposed

algorithm more accurate in thickness variation detection. Then, sensitivity of the biosensor was determined on microarray platforms. Next, differences of the label free biosensor *vs.* FRET were demonstrated. Finally, combined with specific DNA ligation, a mutation experiment for lung cancer detection was presented.

2.1 Chemicals and equipment

All oligonucleotides were synthesized by basic phosphoramidite chemistry and purified by high-performance liquid chromatography (Sangon Biotech, China). The details of all of the oligonucleotides are provided in Table S1 of the supplementary information. Other main chemicals included phosphate buffered saline containing Tween (PBST, 0.05% Tween 20 in phosphate buffered saline) and sodium borohydride solution (1 g sodium borohydride dissolved in 300 mL phosphate buffered saline and 90 mL ethyl alcohol). The spotting buffer, hybridization solution, microarray cleaning liquids I (0.2% SDS in 2× SSC solution) and II (0.2× SSC solution) were all offered by CapitalBio Corporation (China).

The used equipment included a microarray spotter, SmartArrayer-48 (CapitalBio, China), a halogen light, 71PT250 (Saifan, China), a spectrograph, Maya 2000 Pro (Ocean Optics, USA), a 2D nanoscale scanning stage (Physik Instrumente, China) and a three-channel confocal scanner, LuxScan HT24 (CapitalBio, China). Besides, the hybridization box and oven were offered by CapitalBio Corporation (China).

2.2 The interferometric imaging biosensor

The substrate of the DNA chip used in this work was a silica-silicon material. A silica layer on a monocrystalline silicon substrate was modified with aldehyde groups and amino-modified DNA probes fixed on the chip through a Schiff base reaction.

The silicon-silica chip was cut into 4 mm × 4 mm pieces and cleaned in chloroform for 30 min in the dark. Then, the chip was steeped in 0.1 M hydrochloric acid for 30 min and then placed in a 10% HF solution for 1 min. Next, it was immersed in a 1:1:5 (v/v) solution of ammonium hydroxide, hydrogen peroxide, and ultrapure water for 30 min. A 1:1:5 (v/v) solution of hydrochloric acid, hydrogen peroxide, and ultrapure water was used to steep the chip for another 30 min. Then, the chip was steeped in a 2% 3-aminopropyltriethoxysilane solution on a shaking table (220 r/min) for 6 h at 37^{o}C to achieve silanization modification. Finally, a 1% glutaraldehyde solution was used to steep the chip for another 6 h to accomplish the aldehyde modification.

Amino-modified probes were diluted in DNA spotting buffer to fabricate the microarray platforms. The microarrays were spotted using a SmartArrayer-48 microarray spotter, and the spotting diameter was 100 μm with the interval between the spots being 150 μm. After the spotting process, the chip was dried at room temperature for 12 h and immersed in a sodium borohydride solution for 5 min. Then, another wash step was performed with PBST and ultrapure water. Probes were fixed on the chip at one end through the reaction between the amino and aldehyde groups. The schematic of the surface functionalization and probe immobilization is shown in Fig. 1A. In this figure, Fig. 1A-1 and Fig. 1A-2 show the chip after silanization and aldehyde modification, respectively. The sketch of the connection between the surface and the probes is shown in Fig. 1A-3. The postures of the double-stranded DNA molecules and single-stranded probes are shown in Fig. 1A-4.

According to existing research, when double-stranded DNA molecules are fixed at one end, the screw axis forms an approximately 50^{o} angle between the substrate, thus generating a thickness increase [15]. However, single-stranded DNA molecules do not possess rigid structure or

electrostatic interaction between two complementary strands, so their thickness variation is much less than the length of the molecules [16]. When complementary target single-stranded DNA molecules match the probes, the double strand DNA molecules angle upward on the substrate [17,18]. Therefore, a DNA monolayer film forms and generates a thickness increase.

The light reflected by the top surface of the sample layer and the silica-silicon interface results in an interference phenomenon. The interference spectrum can discriminate the thickness variation between the two reflectance layers and then reveal if the DNA hybridization proceed successfully. The simulated spectrums of double-stranded DNA molecules and single-stranded probes are shown in Fig. 1B. In this figure, the green curve represents the simulative spectrums of single-stranded probes, and the blue curve represents the simulative spectrums of double-stranded DNA molecules. It is apparent that the whole interference spectrum red shifts after the hybridization process, indicating a double-stranded structure has formed [8]. To demonstrate the small size of the proposed biosensor, an actual biosensor is shown with a scale label in Fig. 1C.

Insert Figure 1 here.

2.3 Optical setup and data acquisition

To acquire the interference signal of the reflectance spectrum, a detection instrument was designed. A halogen light provided the light source, ranging from 400-1000 nm. An optical system was used to transfer the interference signal to the fiber. A collimated lens helped to generate an alignment beam, which lights the chip through a beam splitter and an objective lens. With a converging lens and an aperture, the spectrum of a microscale spot can be collected by a fiber-spectrometer system. The chip was placed on a 2D nanoscale scanning stage, and thus, the interference spectrum of every pixel could be recorded. Taking the diffraction phenomenon into consideration, the scanning

step was set to 500 nm to guarantee accurate imaging results, and the exposure time was 10 ms. The spectral data were stored and analyzed by a computer. Real-time data processing software was employed to calculate the thickness variation, and a reconstructed image can be exhibited on a screen. The shematic diagram of the setup is shown in Fig. 2.

Insert Figure 2 here.

2.4 DNA hybridization

The complementary target DNA samples were dissolved with hybridization solution. A coverglass was designed with a sample addition hole and a 1.5 mm × 1.5 mm × 1 mm hybridization cavity. The prepared chip was covered by the coverglass and placed in the hybridization box. Before the hybridization process, the hybridization box was heated to 92^{o}C for 2 min. Then, the hybridization box was place in the hybridization oven for 2 h at 60^{o}C. After the hybridization process, the chip was cleaned with microarray cleaning liquids I and II, and then dried with nitrogen gas.

In the experiments, we conducted a series of compliance tests to determine the accuracy and sensitivity of the proposed biosensor. For the accuracy testing, we compared the proposed algorithm with three current methods, including Fast Fourier Transform (FFT) method, spectrum shift method and phase analysis [19-21]. Probes of 8-mer, 16-mer, 32-mer and 64-mer (Cap1, Cap2, Cap3 and Cap4, respectively) were spotted and hybridized with perfectly complementary targets (Tar1, Tar2, Tar3 and Tar4, respectively).The hybridization concentrations were all 1 μM. Four spectrum analysis methods were then applied to measure the thickness variations. All these experiments were repeated 20 times. To prove the accuracy of the measurement results, theoretical values base on discretized worm-like chain model [15] were also calculated.

For the sensitivity testing, 18-mer (Cap6) probes were spotted in a 6 × 6 pattern on the prepared

chip with the spotting concentration of 10 μM. Then, hybridization processes with perfectly complementary targets (Tar6) were performed with the hybridization concentrations of 0.125, 0.25 and 0.5 μM. Another hybridization experiment was employed for the sake of mass sensitivity testing. Probes of 16-mer, 17-mer and 18-mer (Cap2, Cap5 and Cap6, respectively) lengths were spotted in a 6 × 6 pattern and hybridized with perfectly complementary targets (Tar2, Tar5 and Tar6, respectively) at a 0.25 μM concentration. All these experiments were repeated 20 times.

2.5 Weighted spectrum analysis algorithm

Similar to traditional interferometric reflectance imaging biosensors, the thickness variation can be resolved from the equation below [20]:

$$I(k) = (\rho / e)S(k)\delta k\Delta t\{R_r + R_s + 2\sqrt{R_r R_s}\cos[2nk(\Delta x + \delta x)]\} \quad (1)$$

$I(k)$ is the intensity for every wave number of the interference spectrum, k is the wave number, ρ is the detector responsivity, e is the electronic charge, $S(k)$ is the source power density function, δk is the spectral resolution of the spectrometer, Δt is the integral time to acquire an interference spectrum of every pixel, R_r and R_s are the reflectivities of the samples' top surface and the silicon-silica interface, n is the average refractive index of two layers, Δx denotes the thickness of the layer on the silicon substrate before hybridization, and δx accounts for the thickness increase after hybridization. In this work, the refractive index was assumed to be 1.46 according to the related researches [8], and Δx was measured with the method of Wang *et al.* [21]. To simplify the mathematical expression, we defined two variables in following functions:

$$C(k) = (\rho / e)S(k)\delta k\Delta t\left(R_r + R_s\right) \quad (2)$$

$$M(k) = (2\rho / e)S(k)\delta k\Delta t\sqrt{R_r R_s} \quad (3)$$

In this paper, the interference spectrum is treated as an additivity result by a weighted linear model.

Every pixel is regarded as two parts: the silica part and the double-stranded DNA part. Thus, the interference spectrum can be corrected as below abstractly:

$$\begin{aligned} I(k) &= rI_{DNA}(k)+(1\text{-}r)I_{\text{Silica}}(k) \\ &= r\{C(k)+M(k)\cos[2\,\mathrm{n}\,k(\Delta x+\delta x)]\}+(1\text{-}r)\{C(k)+M(k)\cos[2\,\mathrm{n}\,k(\Delta x)]\} \\ &= C(k)+M(k)\{(1\text{-}r)\cos[2\,\mathrm{n}\,k(\Delta x)]+r\cos[2\,\mathrm{n}\,k(\Delta x+\delta x)]\} \end{aligned} \quad (4)$$

Where $I_{DNA}(k)$ is the interference signal of the DNA part and $I_{\text{Silica}}(k)$ is the interference signal of the silica part. δx is the thickness increase due to the double-stranded DNA portions and r is the spectrum proportion of the double-stranded DNA portions. With this strategy, the chip is separated into two parts and only the thickness increase caused by the double-stranded DNA molecules is helpful to reconstruct the image. Different from the current algorithms, the thickness variations are free to the interference of the substrate and the probes, thus the detection will be more accurate and sensitive.

After the hybridization process, a scanning task was performed to record $I(k)$ and determine r and δx. The problem can be solved by finding the optimal parameters that make the minimum integrated squared error. The two parameters were determined by the traversal method to satisfy the formula below:

$$\arg\min_{(r,\delta x)} \sum_{k} \left| I(k)-C(k)-M(k)\{(1\text{-}r)\cos[2\,\mathrm{n}\,k(\Delta x)]+r\cos[2\,\mathrm{n}\,k(\Delta x+\delta x)]\} \right|^2 \quad (5)$$

Equation 5 is a defined formula, where the operator of "arg min" means to determine r and δx to make the minimum sum of the squared error above. $I(k)$ is the real interference spectrum of each pixel. Since all the parameters are determined before the hybridization except r and δx. We can traverse r from zero to one with a step of 0.001 and traverse δx from zero to 20 with a step of 0.01. The two parameters are confirmed when the sum of the squared error is the lowest value. Then, the image reconstruction can be conducted based on the value of δx at every pixel. Please

note that all the imaging results were disposed with median filtering to get rid of detection noises.

2.6 Fluorescence resonance energy transfer (FRET)

FRET is a classical measurement approach to detect the interval between two fluorophores. In this paper, FRET tests were exploited to verify the effectiveness and accuracy of the proposed biosensor. The fluorophores were Cy3 and Cy5 labels, so the interval was the height of the DNA molecules above the substrate, which is the same value as the thickness variation caused by the double-stranded DNA molecules. The sequences of the probes and targets used in the interferometric detection and FRET detection were both same. The only difference was that the probes were Cy3-modified at their 5' termini, and the targets were Cy5-attached at their 5' termini in the FRET verification experiments.

The FRET efficiency reveals the interval between the fluorophores via the formula below [22]:

$$E=\frac{1}{1+(\frac{R}{R_0})^6} \quad (6)$$

E is the FRET efficiency, R is the interval to be measured, and R_0 is the distance at which energy transfer is 50% efficient. In this work, R_0 was treated as a constant equal to 6.0 nm, which was determined in previous research [23].

To measure the FRET efficiency, a three-channel image scanner was used. The image offers three types of data: the donor data, the acceptor data, and the FRET data.

FRET efficiency can be calculated from the formula below [22]:

$$E=\frac{I_{DA}\text{-}dI_{DD}-aI_{AA}}{I_{DA}-dI_{DD}-aI_{AA}+GI_{DD}} \quad (7)$$

Where I_{DD} is the donor data of the chip, I_{AA} is the acceptor data, and I_{DA} is the FRET data. d, a, and G are compensation coefficients. Before the FRET detection tests, the three

coefficients were acquired with the method of Zhu *et al.* [24]. In the following experiments, d was set to 0.058, a was set to 0.056, and G was set to 0.33.

In 3.3, we compared the proposed method with FRET. Probes of 16-mer (Cap2) were spotted and hybridized with perfectly complementary targets (Taq2). The spotting concentrations ranged from 0.25-2 μM with a step of 0.25 μM and the hybridization concentrations were all 0.25 μM. Then probes of 8-mer, 16-mer, 17-mer, 18-mer, 24-mer, 32-mer and 64-mer (Cap1, Cap2, Cap5, Cap6, Cap3, Cap4 and Cap7, respectively)were spotted and hybridized with perfectly complementary targets (Tar1, Tar2, Tar5, Tar6,Tar3, Tar4 and Tar7, respectively). The spotting concentrations and hybridization concentrations were all 0.25μM. To quantitate the thickness variations with FRET, hybridization experiments were conducted with the same DNA sequences and concentrations but the probes were Cy3 labeled and the targets were Cy5 labeled.

2.7 Hybridization procedure for lung cancer gene point mutation

The target DNA sequences were synthesized, which were designed according to the three types of predominant mutations (CGT → CAT, CGT → CTT, and CGT → CCT) at codon 273 of p53 in lung cancer patients, to detect with the proposed biosensor [25]. The concentrations were all 0.25μM so the samples can be easily extracted from the blood sample using a commercial kit (CapitalBio, China). To obtain specific hybridization results, we exploited the biochemical activity of the *Taq* DNA ligase enzyme [26]. The spotted probe will only be lengthened by the reporter sequence if the probe accurately matches the target DNA. In this experiment, four types of synthesized DNA sequences (Tar8-11) served as the targets. They orderly represented the normal wild genotype and the three mutant genotypes. Four types of probes (Cap8-11) were spotted in a 6×6 pattern, and the sequences were perfectly complementary to one of the four targets. We

prepared four biosensors in total, and each target DNA was added to only one biosensor with the report DNA (Rep) and *Taq* DNA ligase enzyme to conduct the hybridization process. Then, the biosensor was incubated in 0.01 M NaOH for 5 min to remove the unligated DNA molecules and cleaned with 10% PBST and deionized water twice at 92^{o}C. Next, the hybridization strand (Tar12) was added to the chip and another hybridization process was performed to form a double-stranded structure with the probes. The concentrations of the reporter DNA and the target DNA were both 0.25 μM.

3. RESULTS

3.1 Accuracy testing of the weighted spectrum analysis

Here we compared the weighted spectrum analysis algorithm with the current methods to evaluate the accuracy. The experiment procedures were introduced in the second paragraph of 2.4. The statistical data with different algorithms and theoretical values were listed in Table 1. According to the theoretical values, the relative errors of FFT method, spectrum shift method, phase analysis and weighted spectrum analysis were 100%, 89.96%, 88.94% and 4.15% respectively. In addition, the relative standard deviation (RSD) of weighted spectrum analysis was 0.0487, proving the reliability of the method. According to discretized worm-like chain model, the average tilt angle of DNA molecules was 57.3^{o} theoretically [15]. The mean tilt angle was 54.44^{o} in this work, which was extremely close to the theoretical value.

Insert Table 1 here.

3.2 Sensitivity testing on DNA microarray platforms

Here we conducted a series of experiments to determine the detection sensitivity. The experiment procedures were introduced in the third paragraph of 2.4 and the detection results were shown in Fig. 3.

Insert Figure 3 here.

In Fig. 3A, imaging results with the hybridization concentrations of 0.125, 0.25 and 0.5 μM (A-1,A-2 and A-3 orderly) were presented. Only the experiment with 0.125 μM cannot bring about a qualified result. So, it can be concluded that the least hybridization to be detected occurred at 0.25 μM.

In Fig. 3B, imaging results with the hybridization length of 16-mer, 17-mer and 18-mer (B-1, B-2 and B-3 orderly) at 0.25 μM were shown. The mean thickness variations for the 16-mer, 17-mer and 18-mer probes were 4.36 nm, 4.59 nm and 4.89 nm. The mean thickness variations of an n-mer and an (n+1)-mer can be told apart clearly from the results.

3.3 Comparison of the interferometric method and FRET

FRET is a conventional method to measure the distance of two fluorophores and widely used in DNA monolayer detection [22-24]. In order to compare the proposed biosensor with conventional fluorescence methods, a series of experiments based on FRET were conducted. The experiment procedures were introduced in the last paragraph of Section 2.6. In Fig. 4, we demonstrated the thicknesses of the monolayers measured by the two methods and the theoretical values with different spotting concentrations and DNA lengths. The thickness of the monolayers measured by the two methods and the theoretical values with different spotting concentrations were shown in Fig. 4A and the thickness of the monolayers measured by the two methods and the theoretical values with different DNA lengths were shown in Fig. 4B. The bars were the standard deviations.

According to Fig. 4A, the spotting concentrations had slight influences on the proposed biosensor but affected fluorescent results seriously. For the interferometric method, the relative errors of the detection results were all less than 2% and changed unremarkably with the changes in spotting concentration. But the relative errors of the FRET method rose from 0.46% to 3.69%.

In Fig. 4B, compared with FRET, the results of the presented methods were more coincident to the theoretical values. The relative errors of the interferometric detection results were all less than 5%. Similarly, for the FRET methods, the relative errors of 8-mer, 16-mer, 17-mer, 18-mer, 24-mer, 32-mer and 64-mer were 11.06%, 0.46%, 2.82%, 1.23%, 4.45%, 11.51% and 43.33%, respectively. In the supplementary information, the detailed relative errors in Fig. 4 were shown in Table S2.

Insert Figure 4 here.

3.4 Test for lung cancer gene point mutation

Due to the sensitive thickness sensing capability, single nucleotide mismatch could be pointed out combined with specific DNA ligation. To demonstrate the potential application of the proposed biosensor, a single nucleotide mismatch test for a lung cancer gene point mutation was developed. The hybridization procedure was shown in Section 2.7.

Insert Figure 5 here.

Fig. 5A presented the hybridization steps and Fig. 5B presented the spotting pattern. The c1 spots are for the normal wildtype genotype, while the c2, c3, and c4 spots represent the CGT → CAT, CGT → CTT, and CGT → CCT mutant genotypes. The final detection results are shown in Fig. 5C-F. For Fig. 5C, the complementary sequence of the normal wildtype genotype (Tar8) was added. For Fig. 5D-F, the complementary sequence of the CGT → CAT mutation (Tar9), CGT → CTT mutation (Tar10) and CGT → CCT mutation (Tar11) was added respectively.

The average thickness increases of the double-stranded DNA molecules (red spots) in Fig. 5C-F were 7.69 nm, 7.59 nm, 7.61 nm and 7.52 nm respectively, while the average thickness increases of the blue spots were 0.91 nm, 0.83nm, 0.93 nm and 0.87 nm respectively. From the experiment results, thicker spots and thinner spots could be distinguished clearly. The thicker DNA monolayers indicated that the spotted probes accurately matched the targets, and thus, single point mutations could be detected.

4. DISCUSSION

According to Section 3.1, it is obvious that weighted spectrum analysis algorithm is much more accurate than the other three methods. The main reason is that the chip is treated as two parts in the proposed algorithm. Only the thickness increase caused by the double-stranded DNA molecules is helpful to reconstruct the image. For the other three algorithms, the phase analysis and spectrum shift method both assume the surface of the exposure area is totally flat [19,20]. In this context, the thickness of the double-stranded DNA molecules is averaged by the substrate and the probes, so the detection result is less accurate at low concentrations. The FFT method considers the peak location after Fast Fourier transformation [21]. However, the noise interference signal exists in the transformation results, so the peak due to the double-stranded DNA molecules was hidden by the noise and cannot be obtained clearly when the concentration is too low. Therefore, in the four label-free detection algorithms, only the proposed method performed well with low concentrations.

Generally, the molecular mass of the target DNA was approximately 324.5 g/mol for each nucleotide [27]. In this work, every pixel of the reconstructed images represented a 500 nm × 500

nm area of the biosensor and the thickness of the hybridization cavity was 1 mm, so the detection limit could be calculated with the formula below:

$$500\times10^{-9}\,\mathrm{m}\times500\times10^{-9}\,\mathrm{m}\times10^{-3}\,\mathrm{m}\times10^{3}\,\mathrm{L/m^3}\times0.25\times10^{-6}\,\mathrm{mol/L}\times324.5\,\mathrm{g/mol}=20.28125\,\mathrm{ag}\approx20\,\mathrm{ag} \quad (8)$$

Also, we could conclude that the sample consumption per unit area of the target DNA content was only 62.5 zm, with the volume of 0.25 pL.

Here we chose mass sensitivity to assess the detection limit because this parameter indicated the concentration, reaction volume and the DNA length concurrently. Compared with conventional interferometric DNA biosensors, the proposed method improved the detection limit in concentration from 20 μM to 0.25 μM. Moreover, the hybridization process could be conducted in a cavity with 0.25 pL per pixel. Thus the sample consumption was reduced significantly. In addition, the proposed biosensor could tell the difference between an n-mer and an (n+1)-mer, which proves the accurate and sensitive thickness detection.

In Fig. 4, as the spotting concentration increased, redundant intermolecular FRET phenomenon occurred since the probes were more than the targets. The intermolecular FRET enhanced the energy transfer between the double strands and increased the FRET efficiency. So the thickness variations were decreased inevitably [22]. However, due to the weighted spectrum analysis strategy, the interferometric method considered the mixed reflected spectrum theoretically thus could point out the accurate thickness variation. So the veracity was not affected by the concentrations. In Table 2, the relative error of 8-mer was much larger than the interferometric method. This is because the theoretical distance between the two strands was only 2.17 nm and the FRET efficiency was more than 96% [28]. The sensitivity was limited since the efficiency was too close to one hundred percent. Moreover, the relative errors of 32-mer and 64-mer were 11.5% and

43.3%. The reason is that FRET can be used as an optical ruler to measure distances less than 10 nm [29]. Since the thicknesses of the monolayers were too large (close to or more than 10 nm), the range limitation of FRET led to coarse detection results. For the interferometric method, the detection range depended on the coherent scope, which was more than 1 μm according to pertinent literatures [21].

5. CONCLUSIONS

In conclusion, a strategy to enhance the sensitivity of interferometric imaging biosensors has been described by providing a weighted spectrum analysis method to detect the nanoscale thickness variations caused by double-strand DNA molecules, thus producing a biosensor that is able to detect very low amounts of target DNA (20 ag). The relative error of thickness detection is merely 4.15%. The hybridization detection can be achieved with even single base pair distinction in length. The high precision and sensitivity demonstrate potential application for gene sequencing and single nucleotide polymorphisms. Compared with the conventional FRET method, the proposed biosensor was more stable, accurate and had wider detection range. A single nucleotide mismatch experiment for lung cancer detection proved the practicality, specificity, and multiplex ability of the device. The biosensor is highly sensitive and consumes minimal sample, making it beneficial for medical purposes and suitable for qualitative detection in medical or clinical examinations.

ACKNOWLEDGEMENTS

This work was supported by the National Natural Science Foundation of China (81327005, 61361160418, 61575100), the National Foundation of High Technology of China (2012AA020102, 2013AA041201), the National Key Foundation for Exploring Scientific Instruments

(2013YQ190467), the Beijing Municipal Natural Science Foundation (4142025), the Beijing Lab Foundation, and the Tsinghua Autonomous Research Foundation (2014Z01001).

APPENDIX A. SUPPLEMENTARY INFORMATION

The following are supplementary information to this article:

References

[1] B.B. Song, H. Zhang, B. Liu, W. Lin, J.X. Wu, Label-free in-situ real-time DNA hybridization kinetics detection employing microfiber-assisted Mach-Zehnder interferometer, Biosens. Bioelectron. 81 (2016) 151-158.

[2] J.K. Chen, G.Y. Zhou, C.J. Chang, C.C. Cheng, Label-free detection of DNA hybridization using nanopillar arrays based optical biosensor, Sensor Actuat. B-Chem. 194 (2014) 10-18.

[3] Y.H. Guo, Q.M. Chen, Y.T. Qi, Y.F. Xie, H. Qian, W.R. Yao, R.J. Pei, Label-free ratiometric DNA detection using two kinds of interaction-responsive emission dyes, Biosens. Bioelectron. 87 (2017) 320-324.

[4] Y. Wang, J. Wang, F. Yang, X.R. Yang, Probing Biomolecular Interactions with Dual Polarization Interferometry: Real-Time and Label-Free Coralyne Detection by Use of Homoadenine DNA Oligonucleotide, Anal. Chem. 84 (2012) 924-930.

[5] R. Jenison, S. Yang, A. Haeberli, B. Polisky, Interference-based detection of nucleic acid targets on optically coated silicon, Nat. Biotechnol. 19 (2001) 62-65.

[6] F. Prieto, B. Sepulveda, A. Calle, A. Llobera, C. Dominguez, A. Abad, A. Montoya, L.M. Lechuga, An integrated optical interferometric nanodevice based on silicon technology for biosensor applications, Nanotechnology 14 (2003) 907-912.

[7] T. Gao, L.J. Rothberg, Label-free sensing of binding to Microarrays using brewster angle straddle interferometry, Anal. Chem. 79 (2007) 7589-7595.

[8] E. Ozkumur, S. Ahn, A. Yalcin, C.A. Lopez, E. Cevik, R.J. Irani, C. DeLisi, M. Chiari, M.S. Unlu, Label-free microarray imaging for direct detection of DNA hybridization and single-nucleotide mismatches, Biosens. Bioelectron. 25 (2010) 1789-1795.

[9] E. Ozkumur, J.W. Needham, D.A. Bergstein, R. Gonzalez, M. Cabodi, J.M. Gershoni, B.B.

Goldberg, M.S. Unlu, Label-free and dynamic detection of biomolecular interactions for high-throughput microarray applications, P. Natl. Acad. Sci. USA 105 (2008) 7988-7992.

[10] L. Moiseev, M.S. Unlu, A.K. Swan, B.B. Goldberg, C.R. Cantor, DNA conformation on surfaces measured by fluorescence self-interference, P. Natl. Acad. Sci. USA 103 (2006) 2623-2628.

[11] X.R. Zhang, G.G. Daaboul, P.S. Spuhler, P. Droge, M.S. Unlu, Quantitative characterization of conformational-specific protein-DNA binding using a dual-spectral interferometric imaging biosensor, Nanoscale 8 (2016) 5587-5598.

[12] X.R. Zhang, G.G. Daaboul, P.S. Spuhler, D.S. Freedman, A. Yurt, S. Ahn, O. Avci, M.S. Unlu, Nanoscale characterization of DNA conformation using dual-color fluorescence axial localization and label-free biosensing, Analyst 139 (2014) 6440-6449.

[13] G.L. Huang, Q. Huang, L. Ma, X.B. Luo, B. Pang, Z.X. Zhang, R.L. Wang, J.Q. Zhang, Q. Li, R.X. Fu, J.C. Ye, fM to aM nucleic acid amplification for molecular diagnostics in a non-stick-coated metal microfluidic bioreactor, Sci. Rep. 4 (2014)7344(1-9).

[14] A. Kussrow, C.S. Enders, D.J. Bornhop, Interferometric Methods for Label-Free Molecular Interaction Studies, Anal. Chem. 84 (2012) 779–792.

[15] J. Ambia-Garrido, A. Vainrub, B.M. Pettitt, A model for structure and thermodynamics of ssDNA and dsDNA near a surface: A coarse grained approach, Comput. Phys. Commun. 181 (2010) 2001-2007.

[16] S. Wenmackers, S.D. Pop, K. Roodenko, V. Vermeeren, O.A. Williams, M. Daenen, O. Douheret, J. D'Haen, A. Hardy, M.K. Van Bael, K. Hinrichs, C. Cobet, M. vandeVen, M. Ameloot, K. Haenen, L. Michiels, N. Esser, P. Wagner, Structural and optical properties of DNA layers covalently attached to diamond surfaces, Langmuir 24 (2008) 7269-7277.

[17] R. Lenigk, M. Carles, N.Y. Ip, N.J. Sucher, Surface characterization of a silicon-chip-based DNA microarray, Langmuir 17(2001) 2497-2501.

[18] J. Ambia-Garrido, A. Vainrub, B. Montgomery Pettitt, Free energy considerations for nucleic acids with dangling ends near a surface: a coarse grained approach, J. Phys.-Condens. Mat. 23 (2011) 325101.

[19] T.Z. Wang, L.P. Xie, H.L. Huang, X. Li, R.L. Wang, G. Yang, Y.N. Du, G.L. Huang, Label-free biomolecular imaging using scanning spectral interferometry, Chin. Opt. Lett. 11 (2013)

111102-111105.

[20] M.A. Choma, A.K. Ellerbee, C.H. Yang, T.L. Creazzo, J.A. Izatt, Spectral-domain phase microscopy, Opt. Lett. 30 (2005) 1162-1164.

[21] T.Z. Wang, Q. Li, X. Li, S.M. Zhao, Y. Lu, G.L. Huang, Use of hyperspectral imaging for label-free decoding and detection of biomarkers, Opt. Lett. 38 (2013) 1524-1526.

[22] J. Zhu, Y. Lu, C. Deng, G.L. Huang, S.Y. Chen, S.K. Xu, Y. Lv, K. Mitchelson, J. Cheng, Assessment of Fluorescence Resonance Energy Transfer for Two-Color DNA Microarray Platforms, Anal. Chem. 82 (2010) 5304-5312.

[23] F.B. Xie, J. Zhu, C. Deng, G.L. Huang, K. Mitchelson, J. Cheng, General and reliable quantitative measurement of fluorescence resonance energy transfer using three fluorescence channels, Analyst 137 (2012) 1013-1019.

[24] J. Zhu, C. Deng, G.L. Huang, S.K. Xu, K. Mitchelson, J. Cheng, Quantitative Fluorescence Correction Incorporating Forster Resonance Energy Transfer and Its Use for Measurement of Hybridization Efficiency on Microarrays, Anal. Chem. 81 (2009) 1426-1432.

[25] J.Q. Zhang, R.X. Fu, L.P. Xie, Q. Li, W.H. Zhou, R.L. Wang, J.C. Ye, D. Wang, N. Xue, X. Lin, Y. Lu, G.L. Huang, A smart device for label-free and real-time detection of gene point mutations based on the high dark phase contrast of vapor condensation, Lab Chip 15 (2015) 3891-3896.

[26] L.P. Xie, T.Z. Wang, T.Q. Huang, W. Hou, G.L. Huang, Y.A. Du, Dew inspired breathing-based detection of genetic point mutation visualized by naked eye, Sci. Rep. 4 (2014).

[27] R.J. Lander, M.A. Winters, F.J. Meacle, B.C. Buckland, A.L. Lee, Fractional precipitation of plasmid DNA from lysate by CTAB, Biotechnol. Bioeng. 79 (2002) 776-784.

[28] V.V. Didenko, DNA probes using fluorescence resonance energy transfer (FRET): designs and applications, Biotechniques 31 (2002) 1106.

[29] Z.G. Zhou, M.X. Yu, H. Yang, K.W. Huang, F.Y. Li, T. Yi C.H. Huang, FRET-based sensor for imaging chromium(III) in living cells, Chem. Commun. 29 (2008) 3387-3389.

Fig. 1. The schematic (A), simulated spectrums (B) and actual photo of the biosensor (C).

Fig. 2. Schematic diagram of the sensor setup.

Fig. 3. Sensitivity testing results on DNA microarray platforms.

Fig. 4. Comparison of the interferometric method and FRET with different spotting concentrations (A) and different DNA lengths (B).

Fig. 5. Sketch (A), spot pattern (B) and detection results (C-F) of the single point mutation test.

Table 1.Different analysis methods to detect the average thickness variations.

Method / DNA length (nm)	FFT method	Spectrum shift method	Phase analysis	Weighted spectrum analysis	Theoretical value
8-mer	0 ± 0	0.22 ± 0.33	0.25 ± 0.32	2.26 ± 0.11	2.17
16-mer	0 ± 0	0.59 ± 0.41	0.64 ± 0.36	4.36 ± 0.12	4.34
24-mer	0 ± 0	0.82 ± 0.64	0.93 ± 0.38	6.65 ± 0.14	6.52
32-mer	0 ± 0	1.34 ± 0.72	1.41 ± 0.47	8.77 ± 0.22	8.69

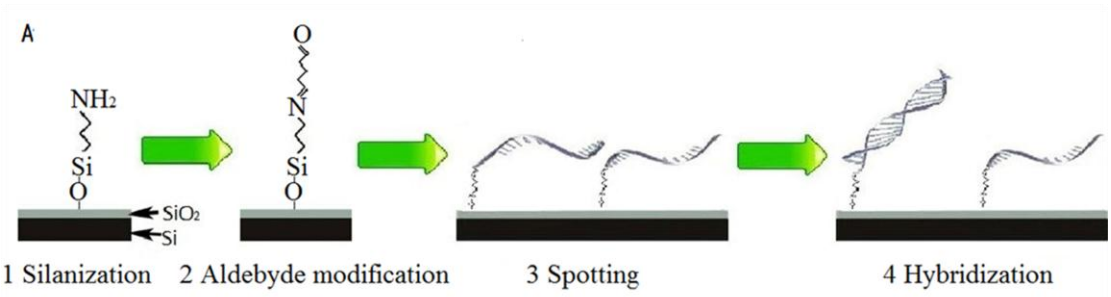
A
NH2
Si
O
SiO2
Si
O
N
Si
O
1 Silanization
2 Aldebyde modification
3 Spotting
4 Hybridization

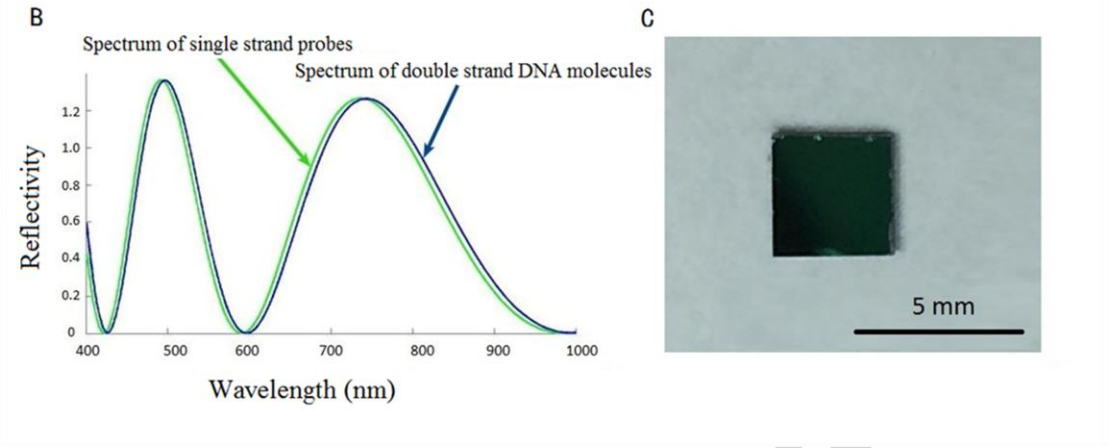
B
Spectrum of single strand probes
Spectrum of double strand DNA molecules
Reflectivity
1.2
1.0
0.8
0.6
0.4
0.2
0
400
500
600
700
800
900
1000
Wavelength (nm)
C
5 mm

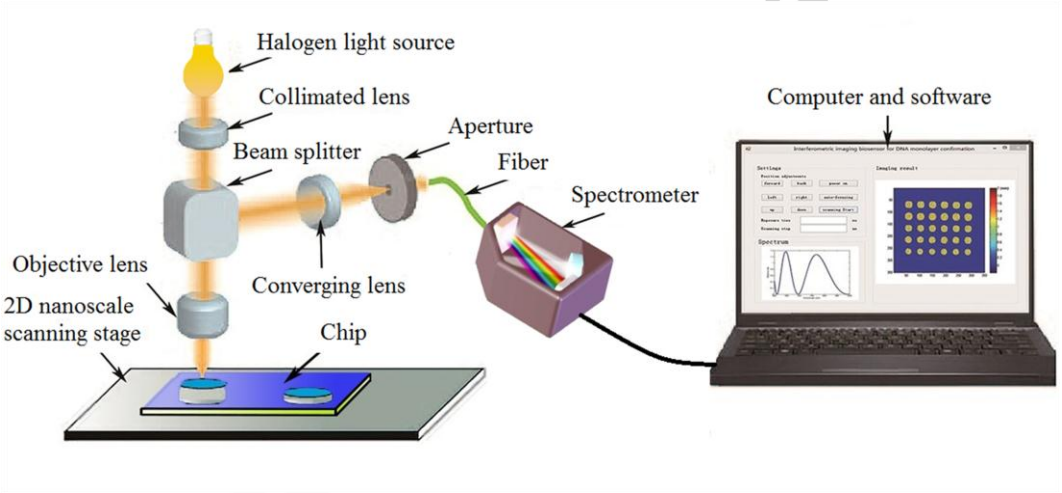
Halogen light source
Collimated lens
Beam splitter
Aperture
Fiber
Spectrometer
Computer and software
Objective lens
2D nanoscale
scanning stage
Converging lens
Chip

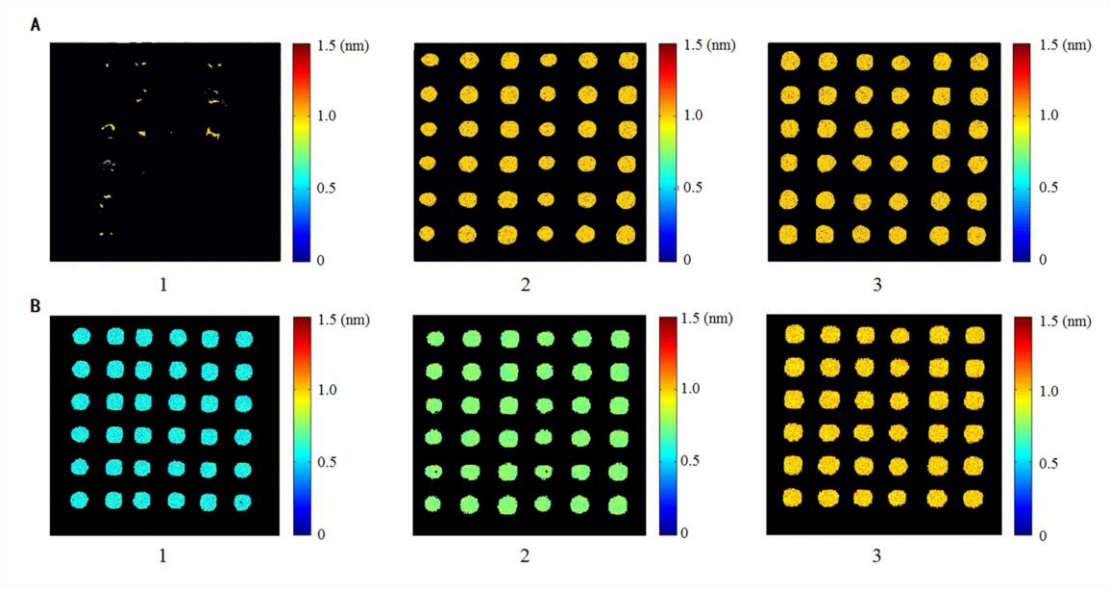
A
1.5 (nm)
1.0
0.5
0
1
2
3
B
1.5 (nm)
1.0
0.5
0
1
2
3

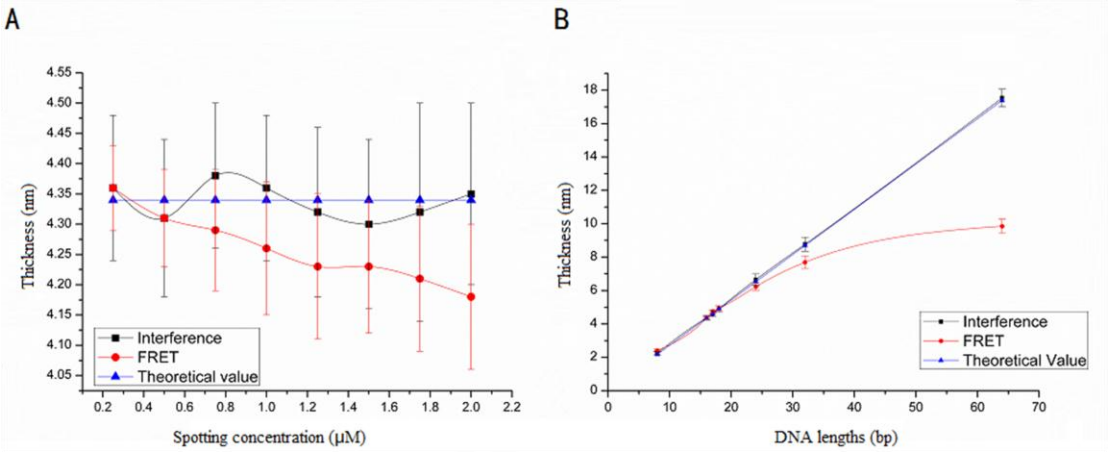
A
Thickness (nm)
Interference
FRET
Theoretical value
Spotting concentration (μM)
B
Thickness (nm)
Interference
FRET
Theoretical Value
DNA lengths (bp)

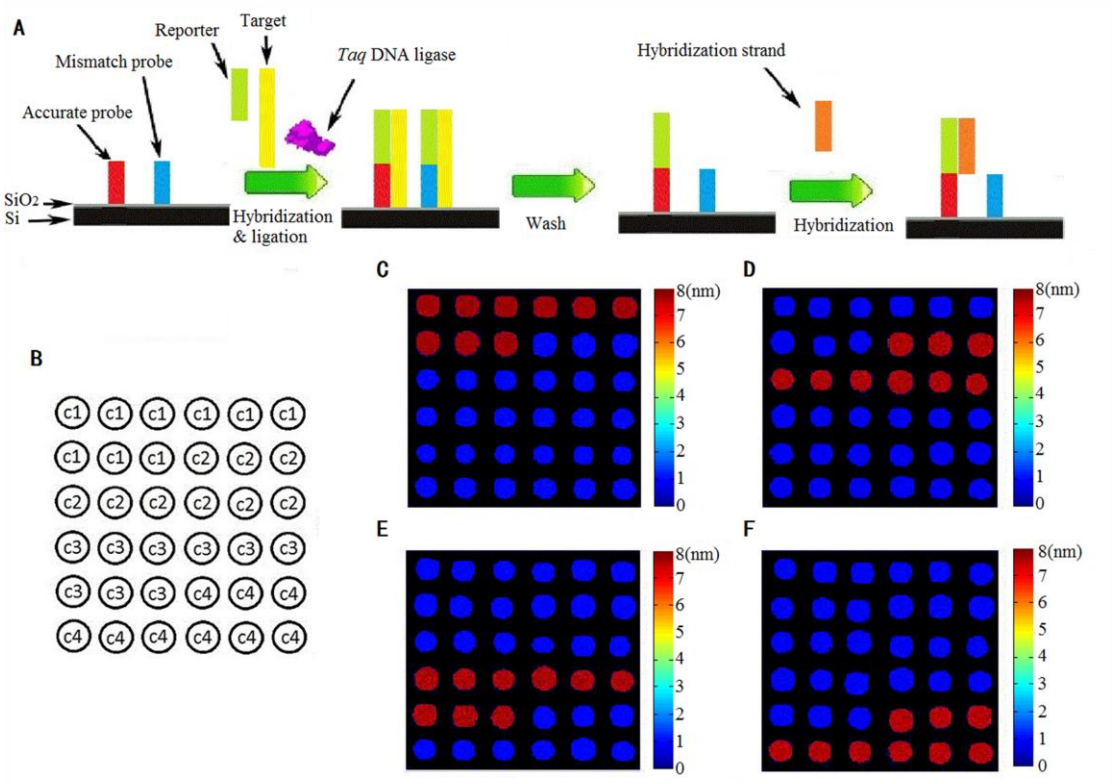

Highlights

- A weighted interferometric biosensor is presented to confirm DNA monolayer films.
- The relative error of thickness detection was reduced from 88.94% to merely 4.15%.
- The mass sensitivity per unit area of the proposed biosensor reached 20 attograms.
- The measurement veracity is free to the changes in spotting concentration and DNA length.
- Single nucleotide mismatch could be pointed out with the biosensor.